Spatial Correlation Analysis of Atrial Activation Patterns during Sustained Atrial Fibrillation in Conscious Goats

B.P.T. Hoekstra[1], C.G.H. Diks[2], M.A. Allessie[3] and J. DeGoede[4]

Archives of Physiology and Biochemistry 2000, Vol. 108, No. 4, 313–331

[1]Division of Image Processing, Department of Radiology, Leiden University Medical Center, The Netherlands
[2]Center for Nonlinear Dynamics in Economics and Finance, Department of Economics and Econometrics, University of Amsterdam, The Netherlands
[3]Cardiovascular Research Institute Maastricht, Department of Physiology, Maastricht University, The Netherlands
[4]Department of Physiology, University of Leiden, The Netherlands

Address: B.P.T. Hoekstra, Leiden University Medical Center, Division of Image Processing, Department of Radiology, P.O. Box 9600, 2300 RC Leiden, The Netherlands. Tel: +31–71–526 2137; Fax: +31–71–526 6801; Email: B.P.T.Hoekstra@lumc.nl

ABSTRACT

In this study we applied both linear and nonlinear spatial correlation measures to characterize epicardial activation patterns of sustained atrial fibrillation in instrumented conscious goats. It was investigated if nonlinearity was involved in the spatial coupling of atrial regions and to what extent fibrillation was organized in the experimental model of sustained atrial fibrillation (AF) in instrumented goats.

Data were collected in five goats during experiments to convert AF by continuous infusion of cibenzoline. Spatial organization during AF was quantified with the linear spatial cross correlation function and the nonlinear spatial cross redundancy which was calculated using the Grassberger–Procaccia correlation integral. Two different types of correlation were evaluated to distinguish simultaneous interaction from non–simultaneous interaction, for instance resulting from propagation of fibrillation waves. The nonlinear association length and the linear correlation length were estimated along the principal axes of iso–correlation contours in two–dimensional correlation maps of the nonlinear spatial redundancy and the linear spatial correlation function, respectively.

To quantitatively assess the degree of nonlinearity, the association length was also estimated from the linearized spatial redundancy using multivariate surrogate data. The differences between the nonlinear and linearized association lengths indicated that a nonlinear component in the spatial organization of AF predominantly existed in the right atrium. The degree of organization characterized by association length along the short principal axis was higher in the right atrium (15 ± 7 mm) than in the left atrium (8 ± 4 mm). The spatial extension of coherent atrial patches was estimated from a surface of association equal to the area spanned by the principal axes of iso–correlation contours from the redundancy, including the effects from non–simultaneous interaction. Interpreting this area as the spatial domain of a fibrillation wavelet, the results suggest that the mapped region was activated on average by two wavelets in the left atrium and by one wavelet in the right atrium. Therefore, the activation pattern of sustained AF in goats was relatively organized, consistent with type II of AF. It is suggested that the surface of association is a measure of the number of independent wavelets present in the atria during sustained AF, and that larger association lengths result from fewer and larger reentrant circuits.

KEYWORDS: spatial organization, cross correlation, cross redundancy, correlation length, association length, nonlinearity, surrogate data, atrial fibrillation

INTRODUCTION

According to the multiple wavelet hypothesis (Moe, 1962), atrial fibrillation is characterized by a varying number of coexisting fibrillation waves which wander through the atria, continuously changing their course of direction. These propagating waves may extinguish or divide again on encountering tissue which is still refractory. Also, wavelets may combine or collide with neighbouring activation waves. The ongoing creation and annihilation of interacting fibrillation waves generates a disordered, turbulent activation pattern during fully developed AF.

Although Moe and coworkers were able to confirm their ideas using a computer model (Moe et al., 1964), experimental evidence for the multiple wavelet hypothesis has only emerged relatively recently with the development of computerized high–resolution mapping systems. It was demonstrated that fibrillation wavelets continually reenter areas which were previously excited either by themselves, termed leading circle reentry (Allessie et al., 1977), or by other activation waves, i.e. random reentry (Hoffman and Rosen, 1981). Detailed mapping experiments (Allessie et al., 1985; Gray et al., 1996; Ikeda et al., 1996; Kirchhof et al., 1993; Ortiz et al., 1994; Schüssler et al., 1993) as well as high–resolution intraoperative studies (Cox et al., 1991; Holm et al., 1997; Konings et al., 1994) have given further insight into the mechanism of AF and support the hypothesis that multiple reentering wavelets are responsible for the perpetuation of AF.

Electrophysiological studies have suggested however, that fibrillation is not an entirely random process (Roithinger et al., 1998; Wells et al., 1978), and it was shown that activation fronts follow preferential paths of previous excitation, termed linking of activation (Damle et al., 1992; Gerstenfeld et al., 1992). Also, by reconstructing the atrial activation pattern during acetylcholine induced AF in the isolated canine heart, it was demonstrated that four to six fibrillation waves are needed on the average for the perpetuation of AF (Allessie et al., 1985), which may indicate an underlying spatial organization. The random nature of fibrillation was further questioned in recent computer simulations and experiments in the isolated rabbit heart (Gray et al., 1995; Jalife and Gray, 1996), in which a single rapidly drifting reentrant spiral wave of excitation generated electrocardiograms displaying a highly irregular morphology characteristic of fibrillation. The corresponding power spectra were narrow–banded suggesting an unsuspected amount of organization.

The complexity of cardiac activation during fibrillation is partly characterized by the spatial extension of coherent myocardial regions and the degree of the underlying organization is quantified by estimating the spatial correlation length in cardiac activation patterns. To this end, cross correlation techniques (Bayly et al., 1993b; Botteron and Smith, 1995; Clayton et al., 1995) and cross spectral analysis (Ropella et al., 1989; Sahakian et al., 1990; Sih et al., 1995) have been applied to multiple electrograms recorded during atrial and ventricular fibrillation. Spatial coherence estimated in the frequency domain was used to differentiate atrial and ventricular arrhythmias from sinus rhythm and it was suggested that algorithms using this measure may improve automatic detection of fibrillation by implantable anti–tachycardia devices (Ropella et al., 1990; Slocum et al., 1988). Furthermore, short–term prediction has been applied to characterize organization during AF (Sih et al., 1999). However, these methods are sensi-

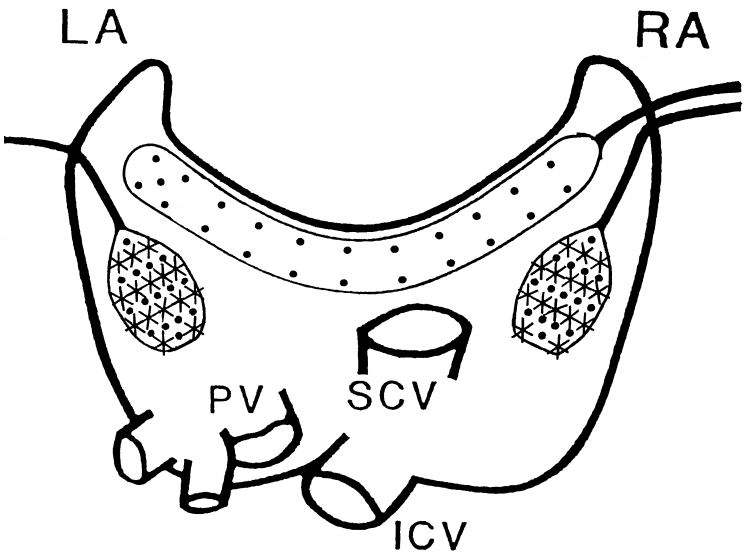

Figure 1: Configuration of the implanted atrial epicardial electrodes. A felt strip containing 23 electrodes was positioned along the bundle of Bachmann (electrode distance 6–10 mm). Two other strips, each containing 30 electrodes, were sutured to the left and right atrial free wall. (electrode distance 4.0–5.7 mm). Electrodes selected for the spatial correlation analysis are indicated by asterisks. LA, left atrium; RA, right atrium; PV, pulmonary veins; SCV, superior caval vein; ICV, inferior caval vein.

tive only to linear aspects contained in the dynamics. Since the heart is a nonlinear excitable medium (Gray and Jalife, 1996; Gray and Jalife, 1998), nonlinear features may be anticipated in cardiac excitation patterns.

Currently, it is unknown to what extent the degree of the spatial organization during AF is governed by linear or nonlinear interactions in the cardiac myocardium. Therefore, in this study both the linear spatial cross correlation function and the nonlinear spatial cross redundancy were estimated to characterize epicardial activation patterns during chronic AF and it was investigated to what extent nonlinearity was involved in the spatial coupling of atrial regions during AF.

MATERIALS AND METHODS

Data Acquisition

Experiments were performed in five goats in which sustained atrial fibrillation (duration $>$ 24 hours) was induced through continuous maintenance of AF by an external automatic fibrillation pacemaker (Wijffels et al., 1995). The goats were instrumented with two felt strips (3.2 cm $\times$ 2.8 cm) sutured to the left and right atrial lateral wall. The strips each contained 30 electrodes (silver, diameter 1.5 mm; electrode distance 4.0–5.7 mm). Furthermore, a strip (10 cm $\times$ 1.2 cm) containing 23 electrodes (electrode distance 6–10 mm) was positioned along Bachmann's bundle and fixed to both atrial appendages. The configuration of the implanted atrial unipolar electrodes is shown in Fig. 1. Electrograms were subsequently amplified (gain 300 to 600),

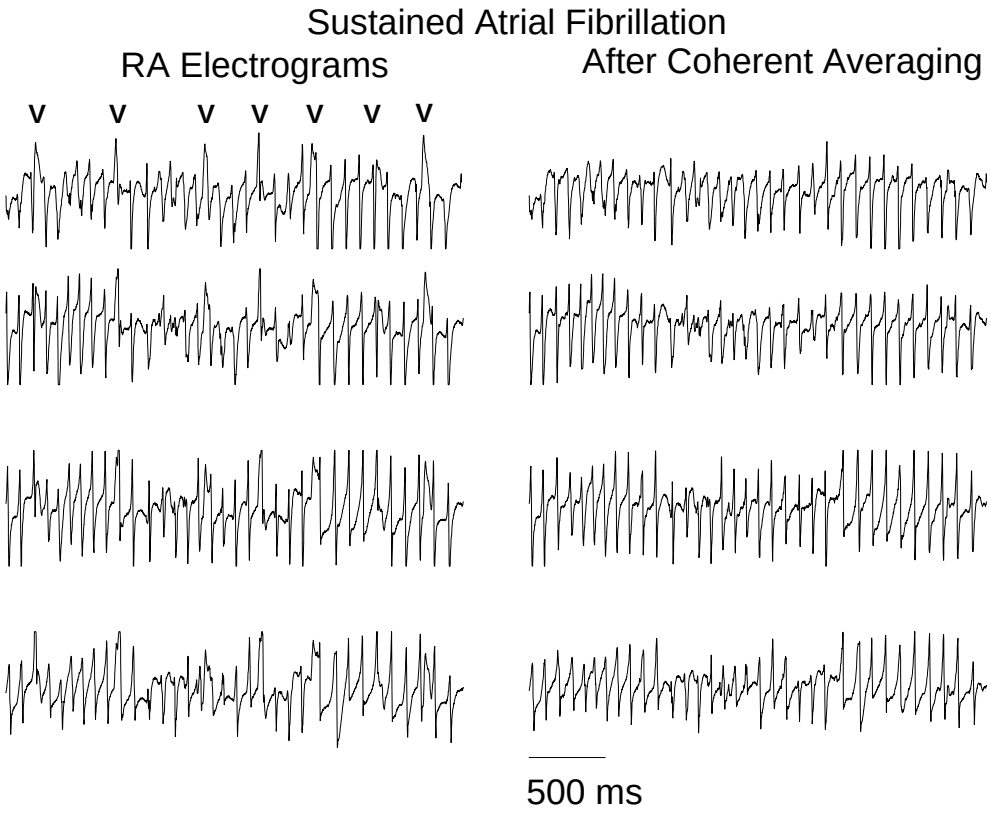

Figure 2: Left panel: unipolar right atrial epicardial (RA) electrograms recorded from a row of electrodes (separation 8 mm) during sustained atrial fibrillation (goat no. 2). The mean fibrillation interval was 96 ms. V, ventricular complex. Right panel: Cleaned electrograms after ventricular deflections were removed by coherent averaging. The morphology of the cleaned electrograms consisted predominantly of single potentials, characteristic of rapidly conducting fibrillation waves.

filtered (1 to 500 Hz), multiplexed (sampling frequency 1 kHz) and AD converted (resolution 8 bits).

Data Selection

Sets of fifteen unipolar epicardial electrograms of one minute duration were simultaneously recorded from the left and right atrial free wall. Fig. 1 depicts the selected electrode matrix used for the spatial correlation analysis (positions indicated by an asterisk). In case measurement noise or artifacts were observed in an electrogram of the matrix, a neighbouring electrode was selected.

Unipolar electrodes positioned at the atrium also pick up the ventricular electrical field. These far field contributions may introduce a bias in the atrial spatial correlation. Therefore, prior to the correlation analysis ventricular deflections were removed from the AF electrograms by a coherent averaging procedure which has been previously described in detail (Hoekstra et al., 1997). In short, a ventricular electrogram served as a reference to detect the occurrence of R waves in the atrial electrograms. Deflections around the R waves in the AF electrograms were averaged to form a template of the ventricular deflections. Finally, cleaned electrograms were

obtained by subtracting the template of the ventricular potential at the appropriate places in the AF electrograms.

Fig. 2 (left panel) shows four right atrial electrograms (RA) measured during sustained atrial fibrillation (goat no. 2). The recording electrodes were positioned along a row and were separated 8 mm from each other. The mean fibrillation interval during this episode was 96 ms and ventricular complexes were clearly visible in the right atrial epicardial tracings. Ventricular deflections were removed by coherent averaging of the electrograms (Fig. 2, right panel) and the morphology of the cleaned electrograms was characterized most of the time by rapid positive upstrokes, followed by a quick relaxation to the iso–electric baseline without a large degree of fragmentation. These single potentials are characteristic of uniform, rapidly conducting fibrillation waves (Konings et al., 1997).

Spatial Correlation Function

The temporal cross covariance function of the extracellular potential V measured at locations $\vec{x}$ and $\vec{x}+\Delta\vec{x}$ and times t and $t+\tau$, respectively, is defined as

$$R(\Delta\vec{x},\tau) \;=\; \lim_{T\to\infty}\; \frac{1}{2T}\; \int_{-T}^{T} V(\vec{x},t)\cdot V(\vec{x}+\Delta\vec{x},t+\tau)\; dt, \tag{1}$$

assuming stationarity of the electrical activity of the heart and translational invariance, so that Eq. (1) is not dependent on $\vec{x}$. The recording duration T was 60 seconds, and before the calculation of Eq. (1) the mean was subtracted from the electrograms. Furthermore, the cross covariance calculated for each electrode pair was normalized to the product of the standard deviations of the constituting electrograms, so that the cross correlation was estimated as

$$\widehat{R}(\Delta\vec{x},\tau) \;=\; \frac{R(\Delta\vec{x},\tau)}{(R(\Delta\vec{x},0)\cdot R(\Delta\vec{x},0))^{\frac{1}{2}}}. \tag{2}$$

To suppress statistical fluctuations the spatial cross correlation $C(\Delta\vec{x},\tau)$ was obtained by averaging Eq. (2) over all possible shifts of the displacement vector $\Delta\vec{x}$ within the electrode matrix. We considered two different cases, taking $\tau = 0$ and $\tau = \tau_{\max}$, which are discussed separately hereafter.

In case $\tau = 0$, there is no relative time shift between electrograms and the spatial correlation function $C(\Delta\vec{x},0) \equiv C_0(\Delta\vec{x})$ characterizes correlations between simultaneous events. We note that $-1 \le C_0(\Delta\vec{x}) \le 1$ and $C_0(-\Delta\vec{x}) = C_0(\Delta\vec{x})$.

The procedure $\tau = \tau_{\max}$ is analogous to the one followed above, except that now for a given $\Delta\vec{x}$ the first maximum $C(\Delta\vec{x},\tau_{\max}) \equiv C_{\mathrm{m}}(\Delta\vec{x})$ of the temporal cross correlation function at lag $\tau_{\max}$ in the range [-180;180] ms was calculated using steps of 1 ms. This was done for each possible pair of electrodes separated by the given displacement $\Delta\vec{x}$ in the electrode matrix. Finally, the resulting maxima in correlation were averaged over all electrode pairs satisfying $\Delta\vec{x}$. From symmetry considerations it follows that $C(\Delta\vec{x},\tau_{\max}) = C(-\Delta\vec{x},-\tau_{\max})$. The procedure $\tau = \tau_{\max}$ accounts for correlations between non–simultaneous events, introduced for example by propagation of fibrillation waves. Procedure $\tau = 0$, however, will underestimate correlations resulting from two sites exhibiting similar activity, yet occurring at a different time.

Spatial Redundancy

To identify the general (i.e. both linear and nonlinear) spatiotemporal dependency between two time series, we used the spatial cross redundancy (Prichard and Theiler, 1995)

$$I(\Delta\vec{x},\tau,r) \;=\; \log\left(\frac{C(V(\vec{x},t),\; V(\vec{x}+\Delta\vec{x},t+\tau),\; r)}{C(V(\vec{x},t),\; r)\cdot C(V(\vec{x}+\Delta\vec{x},t+\tau),\; r)}\right), \tag{3}$$

where $C(\cdot)$ represents the correlation integral estimated at embedding dimension $m = 1$ (in the denominator) and $m = 2$ (in the numerator), and at a coarse–grained resolution r in reconstructed phase space. We assume stationarity of the electrical activity of the heart and translational invariance, so that Eq. (3) is not dependent on $\vec{x}$.

Prichard and Theiler (1995) discuss the connection of various information theoretic quantities to the generalized (order q) correlation integral used in nonlinear time series analysis (Eckmann and Ruelle, 1985; Pawelzik and Schuster, 1987). They demonstrated that quantities such as entropy and redundancy can be estimated efficiently using correlation integrals. The spatial redundancy Eq. (3) is an example of such a statistic and has its information theoretic analogue in the mutual information in case the first order ($q = 1$) correlation integral is used. Mutual information is sensitive to general (linear and nonlinear) dependencies between two time series, and represents the average amount of information that time series contain about each other.

We used the second order ($q = 2$) Grassberger–Procaccia correlation integral (Grassberger and Procaccia, 1983; Takens, 1983), since it can be estimated unbiasedly and no finite sample size corrections are needed (Grassberger, 1988). The procedure used to estimate the correlation integrals has been described elsewhere (Hoekstra et al., 1997). Here, the time series were down-sampled to 10000 samples, and about 5 % of the total number of distances were calculated at a resolution of 12 divisions per binade. Before calculating the correlation integrals, each time series was rescaled separately such that the difference between its minimum and maximum was one. The correlation integrals were evaluated at a coarse–grained resolution r equal to σ, which is defined as the standard deviation of the time series divided by its peak–to–peak value. The resolution r was averaged over five electrograms homogeneously distributed over the area of the electrode matrix, and was in the range 0.10-0.20 for the five goats analyzed. The redundancy was expressed in units Hartley, using base 10 for the logarithm.

Analogous to the linear spatial correlation function, we defined two types of redundancy. The spatial redundancy $I_0(\Delta\vec{x}) \equiv I(\Delta\vec{x},0,\sigma)$ was estimated by averaging over all possible combinations of the displacement vector $\Delta\vec{x}$ within the electrode matrix. Secondly, like the quantity $C_{\rm m}(\Delta\vec{x})$ for the spatial correlation function, the quantity $I_{\rm m}(\Delta\vec{x}) \equiv I(\Delta\vec{x},\tau_{\max},\sigma)$ was defined as the spatial redundancy where $\tau_{\max}$ refers to the lag corresponding to the first maximum in the redundancy. By considering the redundancy at $\tau = \tau_{\max}$, it can be decided whether two time series are really decoupled or merely shifted in time with respect to each other (van der Stappen et al., 1994).

From symmetry arguments it follows that $I(\Delta\vec{x},\tau_{\max},\sigma) = I(-\Delta\vec{x},-\tau_{\max},\sigma)$. The delay $\tau_{\max}$ was obtained in the range [-180;180] ms with a step size of 6 ms to restrain the computer time. This resolution is roughly equal to the conduction time needed for fibrillation waves to travel the distance between two electrodes (4 mm), assuming a conduction velocity during

sustained AF of about 0.7 m·s^{-1} (Wijffels et al., 2000). Hence, the τ step size is of the order of the time of information transfer between two electrodes, and may thus be considered a proper choice for the time resolution to estimate the redundancy $I_{\mathrm{m}}(\Delta\vec{x})$.

Testing for Linearity using Multivariate Surrogate Data

To assess whether nonlinear spatial correlations are present in activation patterns of atrial fibrillation, the linear and nonlinear correlation measures should be compared. If the shapes of the linear and nonlinear correlation functions are similar and the rate of decay of the spatial correlation does not differ substantially, it may be concluded that linear correlations prevail in the spatial organization of AF. In case considerable discrepancies were found, this would suggest the existence of a nonlinear component in the spatial correlation of the AF activation pattern.

However, since the linear cross correlation and the nonlinear redundancy possess different numerical properties, a quantitative comparison of these measures is not possible. For instance, while the correlation function is dependent on the length of the time series only, the redundancy depends on the choice of the coarse–grained resolution in reconstructed phase space, and on a number of parameters to be specified in the calculation of the correlation integrals.

In order to be able to compare the linear and nonlinear characteristics, we applied the strategy advocated by Paluš who compared redundancies and their linearized versions which characterize only linear structures in the data (Paluš et al., 1993). Apart from a comparison on the qualitative level, it was proposed to incorporate the method of surrogate data (Theiler et al., 1992a; Theiler et al., 1992b) to determine whether differences between the linear and nonlinear correlation measures are statistically significant (Paluš, 1995; Paluš, 1996; Paluš and Novotna, 1994). The method of surrogate data amounts to a quantitative comparison of a convenient nonlinear test statistic calculated for both the measured data and for a number of computer generated surrogate time series, which by construction are realizations of a linear stochastic process. Only in case the value of the test statistic calculated for the original data can be distinguished statistically from the results of the surrogate dataset, the null hypothesis of linearity is rejected and nonlinear properties are assigned to the data.

More specific, the idea is to test against the null hypothesis that the data were generated by a process from within a certain class of linear random models specified by the procedure to generate the surrogate data. Typically, a surrogate time series constructed from a single electrogram has the same first and second order statistics (sample mean and variance) as the observed electrogram, and properties such as the circular autocorrelation function and sample power spectrum are preserved using the method of phase randomization in the frequency domain (Theiler et al., 1992a). Here we follow a recipe (Prichard and Theiler, 1994) to generate multivariate surrogate data, so that the linear cross correlation between electrograms was preserved as well.

Moreover, since it was our aim to estimate a correlation length and not merely test for nonlinearity, we constructed surrogate data which also mimicked the amplitude distribution of the electrograms. Therefore, each surrogate series was amplitude adjusted (Theiler et al., 1992a) to preserve the amplitude distribution of the electrograms. This extends the null to a somewhat broader class of models which includes a monotonous, time independent, nonlinear

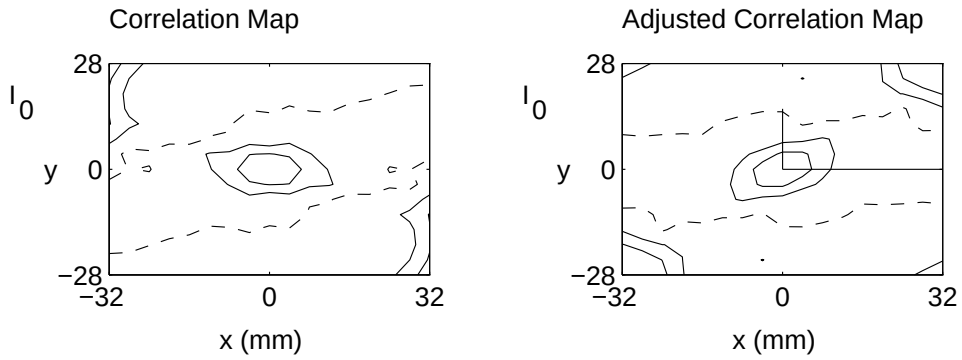

Figure 3: Spatial correlation map of the redundancy I_0 (goat no. 3). After a rotation of the set of redundancy values an adjusted correlation map is obtained (right panel). To account for the anisotropy in the decay of the spatial correlation, the association length was estimated in the direction of the short and long principal axis of the adjusted iso–correlation contours. The short axis length was 15.9 mm, while the long axis length exceeded the border of the mapped region. The estimated association lengths are shown as line segments in the right panel. Iso–correlation contours are drawn in the correlation maps at levels $e^{-\frac{1}{4}}$, $e^{-\frac{1}{2}}$, e^{-1}, e^{-2}, e^{-4} with respect to the maximum value. The e^{-1} contour is plotted as a dashed line and spatial correlation decreased towards the borders of the map.

function which rescales the distribution of Gaussian surrogate time series to the distribution of the electrograms. Consequently, the sample mean and variance are also preserved.

Thus, we tested the null hypothesis that spatial correlation observed in activation patterns of AF was generated by a multivariate linear Gaussian random process in space and time, including the possibility that the amplitude distribution of electrograms was transformed by a monotonous static nonlinear measurement function. The rate of decay of the spatial redundancy (viz. association length) was used as a test statistic to investigate to what extent nonlinearity was involved in the coupling of different atrial regions during AF. To this end, the redundancy estimated from the set of coherent averaged AF electrograms was compared with the redundancy estimated from a set of surrogate electrograms. The latter will be referred to as the linearized redundanc, cf. (Paluš, 1995), hereafter.

Association and Correlation Length

In the subsequent sections the spatial correlation is displayed in correlation maps as a function of the displacement within the electrode matrix. Fig. 3 (left panel) shows a correlation map of the redundancy I_0 estimated for an episode of sustained AF recorded at the right atrium (goat no. 3). The x and y axis were approximately parallel and perpendicular to the AV ring, respectively. The top of the map points in the direction of the AV ring and the bottom is directed towards the atrial appendage.

For instance, the spatial autocorrelation is located at the origin (0, 0) of the correlation map. The value calculated at position (12, -8) corresponds to the average spatial correlation calculated from electrode pairs separated 12 mm in the positive x direction and 8 mm in the negative y direction. The correlation maps are point symmetric with respect to the origin, according to

the symmetry properties of the correlation measures.

The spatial correlation was projected onto iso–correlation contours (MatLab software package, the MathWorks Inc., USA) using an interpolation step of 1 mm (Bayly et al., 1993a). The pattern of spatial correlation was visualized by plotting contours on a logarithmic scale at levels $e^{-\frac{1}{4}}$, $e^{-\frac{1}{2}}$, e^{-1}, e^{-2}, e^{-4} (or 0.78, 0.61, 0.37, 0.14, 0.02) with respect to the maximum (auto)correlation. The e^{-1} contour is plotted as a dashed line and spatial correlation decreased towards the borders of the map.

Since the pattern of correlation contours was in general rather anisotropic, the spatial rate of decay was quantified by calculating a characteristic length in two directions. To this end, the correlation values were rotated and put on principal axes using singular value decomposition (MatLab). This is illustrated in Fig. 3 (right panel) showing the adjusted correlation map after transformation of the correlation data onto principle axes. Next, a characteristic length l was determined from an exponential fit $f(r) = c \cdot e^{-r/l}$ of the adjusted correlation data as a function of distance r along the principal axes, excluding $r = 0$. We refer to the length l as *association length* in case it is estimated from the nonlinear redundancy to distinguish it from the *correlation length* estimated from the linear correlation function. The association length along the short principle axis was 15.9 mm, while the association length along the long principle axis exceeded the border of the mapped region (Fig. 3 right panel, indicated by line segments).

In the following we will show original (i.e. unadjusted) correlation maps so that directional information is preserved in the maps. Furthermore, the e^{-1} contour was used as a reference to compare different types of correlation maps. We will refer briefly to the short and long principle axis of the e^{-1} contour as the short and long axis, respectively. In order to illustrate the differences observed in the various types of correlation maps, the association and correlation length were also compared by taking them equal to the length of the short and long axis.

RESULTS

In the subsequent sections, we present the spatial correlation analysis applied to the coherent averaged electrograms of a representative example (goat no. 3).

Analysis of Right Atrial Activation Patterns

Fig. 4 (upper row) shows right atrial correlation maps of the redundancy measures I_0 and I_m, which were very similar. The length of the long axis of the e^{-1} contour exceeded the border of the mapped area, while the short axis length was 15.9 mm for both I_0 and I_m. In the correlation maps of the linearized redundancy (middle row) the length of the long axis was 15.8 and 20.7 mm for I_0 and I_m respectively. The length of the short axis had diminished to 6.6 (I_0) and 8.2 mm (I_m), indicating that spatial correlation was decaying more rapidly for the surrogate data. Spatial correlation in maps of the linear measure C_0 (Fig. 4, bottom row) decayed rapidly (short axis length 11.2 mm), while the long axis exceeded the border of the mapped region. The e^{-1} contour of C_m had extended with respect to C_0 and the short axis length had been prolonged to 23.5 mm. The long axis estimated from C_0 and C_m exceeded the border of the mapping

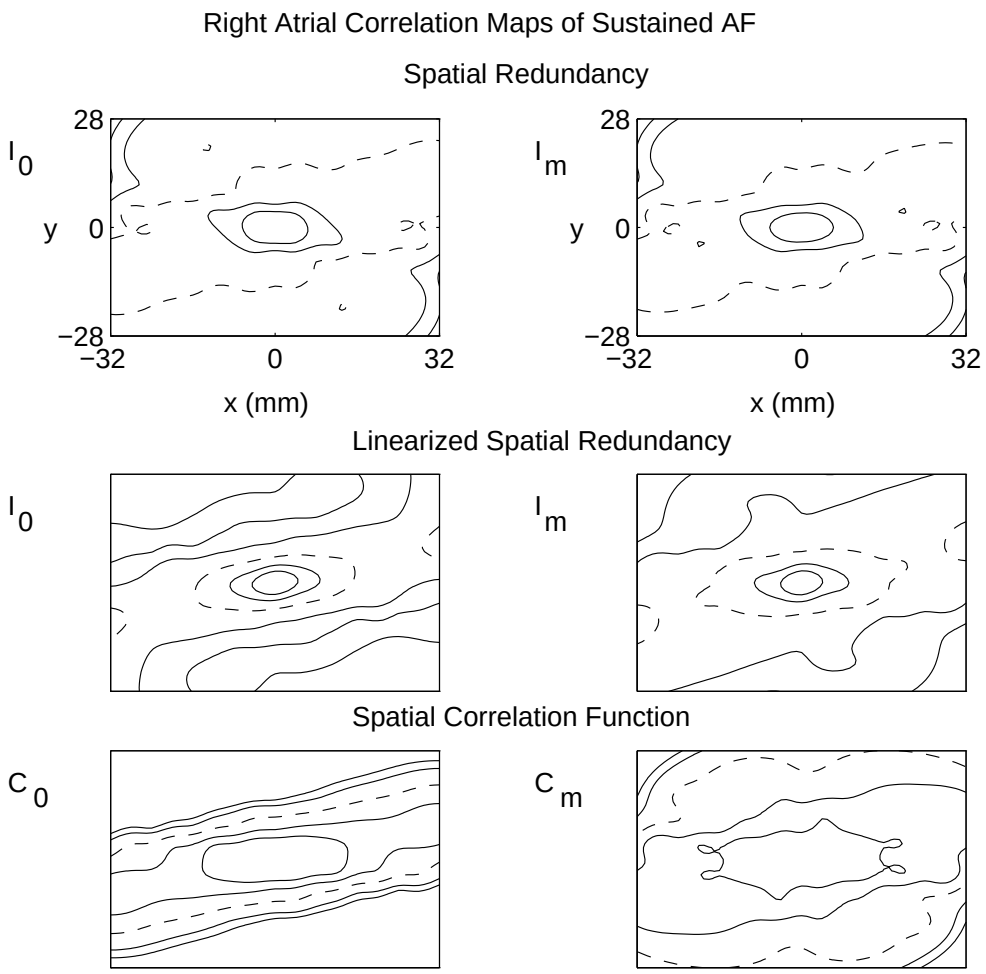

Figure 4: Right atrial correlation maps of sustained atrial fibrillation (goat no. 3). The spatial redundancies I_0 and I_{m} (upper panels) were estimated from the set of coherent averaged electrograms. Surrogate electrograms were calculated to estimate the linearized spatial redundancies (middle panels). Correlation maps of the spatial correlation functions C_0 and C_{m} are shown in the bottom panels. The e^{-1} iso–correlation contour (dashed line) is used as a reference to compare the different correlation maps. See text for further explanation.

electrode.

The association length equal to the short principal axis of the e^{-1} contour in the left and right atrium during sustained AF is summarized in Table 1 for the population of five goats. In the right atrium, there was a substantial difference between the short axis length estimated from $I_0[o]$ (14.1 $\pm$ 6.0 mm) and the linearized redundancy $I_0[s]$ (5.9 $\pm$ 1.0 mm). The symbol $[o]$ refers to the measured electrograms and $[s]$ to the surrogate data. Similar values were observed for the short axis length estimated from $I_{\mathrm{m}}[o]$ and its linearized version $I_{\mathrm{m}}[s]$. The differences in association lengths estimated from I_0 and I_{m} were not substantial for both the original and the linearized redundancy (compare left and right column in Fig. 4).

The right atrial correlation length estimated from $C_0[o]$ was 9.5 $\pm$ 1.7 mm (Table 1). The average maximum correlation length was 20.5 $\pm$ 8.1 mm ($C_{\mathrm{m}}[o]$), taking into account the conduction delay of wave propagation between different right atrial sites. In almost all goats the length of the long axis exceeded the border of the mapped area for both the correlation function

	Association length (mm)	
Redundancy	LA	RA
$I_0[o]$	7.7 (3.4)	14.1 (6.0)
$I_\mathrm{m}[o]$	8.5 (4.4)	14.9 (6.7)
Linearized Redundancy		
$I_0[s]$	5.4 (1.6)	5.9 (1.0)
$I_\mathrm{m}[s]$	5.8 (1.9)	8.2 (4.0)
	Correlation length (mm)	
Cross Correlation	LA	RA
$C_0[o]$	10.4 (3.1)	9.5 (1.7)
$C_\mathrm{m}[o]$	14.9 (7.3)	20.5 (8.1)

Table 1: Association and correlation length equal to the short principle axis of the e^{-1} contour in correlation maps of sustained atrial fibrillation. Results for the spatial redundancy (I_0, I_m) and spatial correlation (C_0, C_m) are presented as Mean (SD). Symbols $[o]$ and $[s]$ refer to the original and surrogate electrograms. LA, left atrium; RA, right atrium.

and the redundancy. The corresponding association and correlation lengths were therefore not tabulated.

The redundancy along the short principal axis of the right atrial correlation map is plotted in Fig. 5 (upper left panel). The short axis curves of I_0 and I_m were clearly different from the surrogate curves (dashed lines). To summarize the data, the spatial redundancy along the short principal axis was fitted with an exponential function. The estimated association length was 18.8 ± 2.4 mm for the curve $I_0[o]$ and 17.8 ± 1.9 mm for $I_\mathrm{m}[o]$ versus 6.2 ± 0.7 mm ($I_0[s]$) and 10.0 ± 0.6 mm ($I_\mathrm{m}[s]$) for the linearized redundancies. The curves I_0 and I_m in the direction of the long principal axis (Fig. 5, upper right panel) were also distinguished from the surrogate curves. However, these curves could not be properly fitted by an exponential function, since the spatial redundancy remained high or fell off slowly along the long axis. The curves C_0 and C_m along the short principal axis are shown in Fig. 5 (lower left panel). The curve C_m, which accounted for propagation of AF activation waves, decreased slowly along the short axis. The spatial correlation C_0 in the direction of the long principal axis (Fig. 5, lower right panel) remained high over the entire distance mapped. The curve C_m along the long axis was practically identical to the correlation curve C_0. No correlation lengths were determined from a fit from the curves C_0 and C_m along the principal axes, since an exponential function was not suited to fit the data.

To check the quality of the surrogate data, short axis curves were also estimated from $C_0[s]$, and the results were identical to the curves obtained from $C_0[o]$. If the linear correlation function would already have indicated differences between the original and surrogate data, the null hypothesis may have been falsely rejected, because nonlinear properties were erroneously intro-

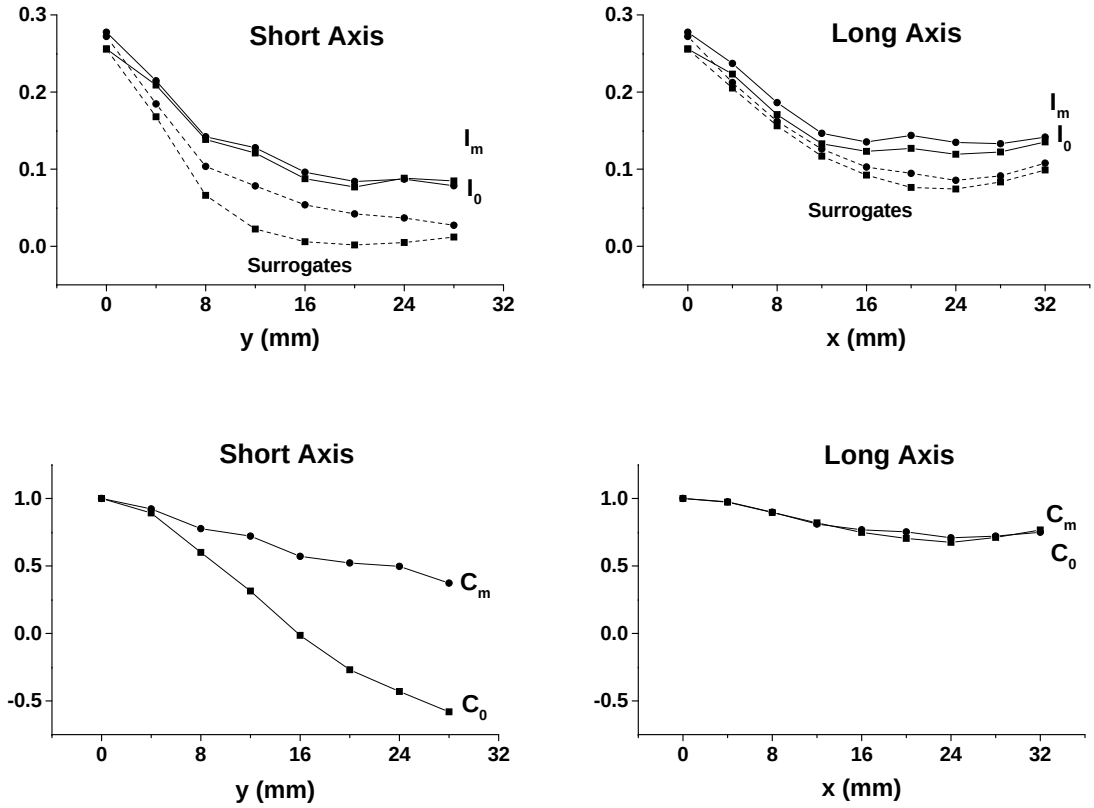

Figure 5: Right atrial correlation curves (goat no. 3) corresponding to the short and long principal axis of the iso–correlation contours. The upper panels illustrate the differences between the spatial redundancies I_0, I_{m} and their linearized versions (dashed lines), so that a nonlinear component was present in the organization of right activation patterns of sustained AF. The lower panels present the results for the linear spatial correlation C_0 and C_{m}. Symbols ■ and • denote the curves estimated at $\tau = 0$ and $\tau = \tau_{\max}$, respectively.

duced during the construction of the surrogate data (cf. (Paluš, 1995), who used the linearized redundancy as a test statistic for the quality of the surrogate data).

Table 2 shows the average association length for the five goats from an exponential fit of the short principal axis in the left and right atrium during sustained AF. In the right atrium, the association length estimated from the redundancy $I_0[o]$ and its linearized version $I_0[s]$ were consistent with the corresponding values estimated from the short axis of the e^{-1} contour (Table 1). This was also the case for the association length estimated from I_{m}.

Analysis of Left Atrial Activation Patterns

Left atrial correlation maps (goat no. 3) of the redundancy are shown in Fig. 6. The contours of the redundancy I_0 (upper row) were elliptically shaped during sustained AF and the short and long axis length was 10.7 and 21.3 mm, respectively. The short (15.9 mm) and long (23.5 mm) axis length estimated from I_{m} were slightly larger. Association lengths estimated from the linearized redundancies (middle row) had decreased to 7.0 mm along the short axis and 15.1 mm in the long axis direction ($I_0[s]$). The results for $I_{\mathrm{m}}[s]$ were 8.2 and 17.2 mm for the short and

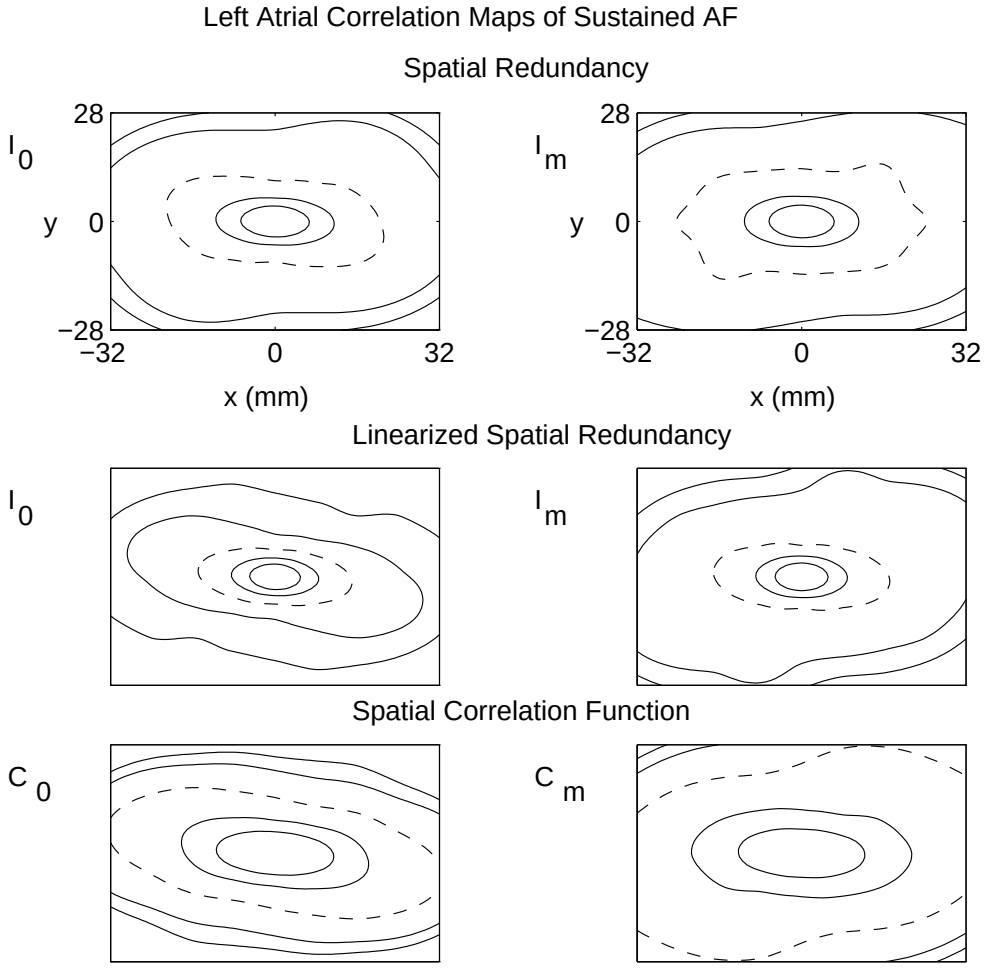

Figure 6: Left atrial correlation maps of sustained atrial fibrillation (goat no. 3) showing the the spatial redundancies I_0 and I_{m} (upper panels) and the corresponding linearized spatial redundancies (middle panels). Correlation maps of the spatial correlation functions C_0 and C_{m} are shown in the bottom panels. The e^{-1} iso–correlation contour (dashed line) is used as a reference to compare the different correlation maps. See text for further explanation.

long axis, respectively. Correlation maps of the linear correlation length (bottom row) showed elongated contours. The long axis of the linear correlation measures exceeded the border of the mapped region and the short axis correlation length was 13.8 (C_0) and 23.8 mm (C_{m}).

The left atrial estimates of the short principal axis length (e^{-1} contour) are presented in Table 1 for all goats. The association length of the redundancy $I_0[o]$ was 7.7 ± 3.4 mm, which was similar to the length estimated for $I_{\mathrm{m}}[o]$ (8.5 ± 4.4 mm). The association length of the linearized redundancy $I_0[s]$ and $I_{\mathrm{m}}[s]$ decreased to 5.4 ± 1.6 and 5.8 ± 1.9 mm, respectively. The correlation lengths for the linear correlation measures were 10.4 ± 3.1 mm ($C_0[o]$) and 14.9 ± 7.3 mm ($C_{\mathrm{m}}[o]$).

Fig. 7 (upper left panel) shows the redundancy I_0 and I_{m} along the short principal axis of the left atrial correlation map. Both curves were distinguished from the corresponding surrogate curves (dashed lines). The association lengths estimated from an exponential fit of the data were 11.7 ± 0.8 mm ($I_0[o]$) and 13.4 ± 0.8 mm ($I_{\mathrm{m}}[o]$), respectively. For the linearized redundancies the fitted short axis lengths were 6.6 ± 0.8 mm ($I_0[s]$) and 9.6 ± 0.7 mm ($I_{\mathrm{m}}[s]$). Hence, also

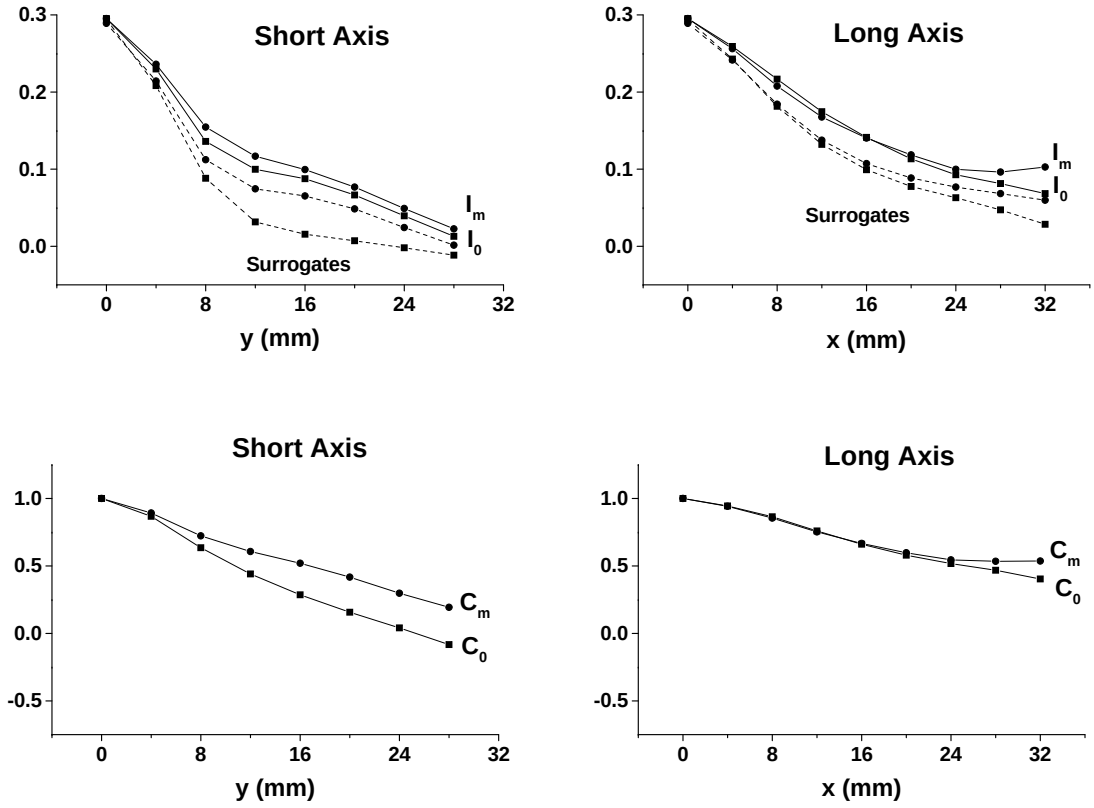

Figure 7: Left atrial correlation curves (goat no. 3) corresponding to the short and long principal axis of the iso–correlation contours. The upper panels show the spatial redundancies I_0, I_m and their linearized versions (dotted lines). The spatial correlation C_0 and C_m is shown in the bottom panels. Symbols ■ and • denote the curves estimated at $\tau = 0$ and $\tau = \tau_\mathrm{max}$, respectively.

in the left atrium the short axis association length was different for the original and surrogate data sets. Also, the curves $I_0[o]$ and $I_\mathrm{m}[o]$ in the direction of the long axis (Fig. 7, upper right panel) were distinguished from the surrogate curves. The redundancy data were not fitted along the long principal axis, since the spatial correlation remained high or decreased slowly. The left atrial correlation curves C_0 and C_m decreased slowly along the short axis (Fig. 7, lower left panel) and remained high in the direction of the long axis (lower right panel). Along both the short and long principal axis, the curves C_0 and C_m could not be fitted properly with an exponential function.

The average association length estimated from an exponential fit of the short principal axis of the correlation map is shown in Table 2 for the five goats in the left atrium. Like in the right atrium, for both $I_0[o]$ and $I_\mathrm{m}[o]$ and the corresponding linearized redundancies, the values from the exponential fit were in close correspondence with the association length estimated from the short axis of the e^{-1} contour (Table 1).

	Association length (mm)	
Redundancy	LA	RA
$I_0[o]$	8.2 (3.6)	15.2 (5.9)
$I_{\mathrm{m}}[o]$	9.2 (4.1)	15.5 (5.5)
Linearized Redundancy		
$I_0[s]$	5.1 (1.6)	5.5 (0.9)
$I_{\mathrm{m}}[s]$	6.4 (2.3)	9.4 (3.6)

Table 2: Association length from an exponential fit of the short principle axis in correlation maps of sustained atrial fibrillation. Results for the spatial redundancy I_0 and I_{m} are presented as Mean (SD). Symbols $[o]$ and $[s]$ refer to the original and surrogate electrograms. LA, left atrium; RA, right atrium.

DISCUSSION

Another test for nonlinearity can also be performed by comparing the nonlinear correlation measure with the redundancy of a multivariate linear Gaussian random process. The spatial redundancy I_0 of a multivariate linear Gaussian random process can be expressed in terms of its spatial correlation function C_0 as

$$I_0(\Delta\vec{x}) = -\frac{1}{2}\ \log\left(1 - C_0^2(\Delta\vec{x})\right), \tag{4}$$

where $\Delta\vec{x}$ denotes spatial displacement. This quantity is analogous to the linearized redundancy for delay embedded time series (Fraser, 1989; Paluš, 1995; Prichard and Theiler, 1995). We note that Eq. (4) holds for the mutual information, which follows from Eq. (3) using the first order ($q = 1$) correlation integral. It has been shown that the generalized (order q) linear redundancies do not depend on q in the case of a linear Gaussian random process (Prichard and Theiler, 1995). In this study $I_0(\Delta\vec{x})$ was estimated using the second order ($q = 2$) correlation integral.

Assuming an exponential spatial decay of the linear correlation C_0 and using a first order approximation for the logarithm, it follows from Eq. (4) that the association length estimated from the redundancy I_0 of a multivariate linear Gaussian random process is a factor two smaller than the correlation length estimated from C_0. Thus, there is a difference in the definition of correlation length depending on the type of correlation measure used: the nonlinear correlation length (association length) is a factor two smaller than the linear correlation length.

In the present study, the redundancy was compared with the linearized redundancy estimated from amplitude adjusted surrogate data (rescaled to the amplitude distribution of the measured data). We noticed that the average association length estimated from $I_0[s]$ was roughly a factor two smaller than the correlation length estimated from $C_0[o]$ (equivalent with $C_0[s]$), see Table 1. Therefore, the effect of a static nonlinearity was probably not large in the comparison of the measured data with randomized surrogate data. It would be interesting to investigate the relation between the association and correlation length for the case of a linear process driven by

non–Gaussian noise.

In general, the different numerical properties of the nonlinear redundancy and the linear correlation function render a quantitative comparison difficult. For example, the redundancy requires the choice of a resolution in phase space, while the linear correlation function depends only on the length of the time series. Pompe et al. (1998) applied both linear and nonlinear correlation measures to study the coupling in the cardiorespiratory system. In particular, heart beat series were correlated with a respiratory signal recorded in a human newborn to characterize different sleep stages. It was found that during quiet sleep the linear correlation attained values up to 0.65, which suggests that the coupling was "rather strong". The second order ($q = 2$) redundancy reached values up to 0.35–0.40 bit, from which it was concluded that the coupling was "rather weak", since it was about 10% of the maximal value. The authors did not make a statement about the relative contribution of the linear and nonlinear component in the cardiorespiratory dynamics. However, when the linear correlation 0.65 is substituted in Eq. (4), the linearized redundancy is 0.40 bit, which is equal to the value found for the nonlinear redundancy. This suggests that the nonlinear interaction between heart rate and respiration was small during quiet sleep.

This example illustrates that it is not always straightforward to interpret the results of a correlation analysis when linear and nonlinear measures with different numerical properties are compared. The method of multivariate surrogate data avoids these complications since the nonlinear correlation measure can be compared unequivocally and quantitatively with its linearized version to test the null hypothesis of linearity. Although it is not without its pitfalls (Chan, 1997; Paluš, 1995; Rapp et al., 1994; Schreiber and Schmitz, 1996; Stam et al., 1998; Theiler et al., 1993; Theiler and Prichard, 1996; Theiler and Prichard, 1997), the method of surrogate data has to be preferred to distinguish linear and nonlinear components in the dynamics of coupled time series.

Finally, we note that the right atrial spatial correlation $C_0[o]$ obtained negative values with increasing distance along the short axis (Fig. 5 lower left panel), whereas the linearized spatial redundancy $I_0[s]$ was about zero at large distances (Fig. 5 upper left panel, dashed lines). This is a consequence of the properties of the linearized redundancy: linear structures look less pronounced because of the logarithmic transformation in Eq. (4). We remark that, in a comparison with the redundancy, the *square* of the correlation function was plotted (Pompe et al., 1998).

Nonlinearity in Activation Patterns of Sustained AF

The difference in the average short axis association length of the redundancy $I_0[o]$ and its linearized version $I_0[s]$ was 9.7 mm in the right atrium and 3.1 mm in the left atrium (Table 2). Likewise, the difference in short axis length estimated from $I_{\mathrm{m}}[o]$ and $I_{\mathrm{m}}[s]$ was 6.1 mm and 2.8 mm in the right and left atrium, respectively. Five sets of surrogate electrograms were constructed for two goats (no. 1 and 2) to check if the differences between the original and linearized association lengths were significant. Since the differences in association lengths between the original and linearized redundancy were markedly larger than the standard deviation of the

association length estimated from the surrogates (about 1 mm for both $I_0[s]$ and $I_{\mathrm{m}}[s]$), we conclude that nonlinear spatial coupling was present in both atria during sustained AF. The difference in average association length between the right and left atrium suggests that a nonlinear component was predominantly involved in the spatial organization of right atrial activation patterns and that the right atrial activation pattern was organized to a higher degree than the left atrium.

Furthermore, the difference in association length between the linearized redundancies $I_{\mathrm{m}}[s]$ and $I_0[s]$ (Table 2) was larger in the right atrium (3.9 mm) than in the left atrium (1.3 mm). Since the difference at least partly accounts for the aspect of wave propagation (i.e. $\tau = \tau_{\max}$ versus $\tau = 0$), local activation in the right atrium was probably more uniform than in the left atrium. This was also evident from the difference in correlation length estimated from $C_{\mathrm{m}}[o]$ and $C_0[o]$, which was 11.0 mm in the right atrium and 4.5 mm in the left atrium (Table 1).

Spatial Correlation during Sustained Atrial Fibrillation

The correlation function C_0 has been used to quantify spatial order in high–density maps of electrically induced ventricular fibrillation (VF) in pigs and the estimated correlation length was 4 to 10 mm (Bayly et al., 1993b). Sih et al. (1995) used a spectral analysis approach and characterized spatial organization with the magnitude squared coherence (Ropella et al., 1989). An alignment procedure was used to correct for a time lag between signals, and the estimated correlation length in epicardial maps of induced VF in pigs was 5 to 10 mm, which is consistent with the results reported by Bayly et al. (1993b). These results point out that the mechanism of ventricular fibrillation, often referred to as random reentry (Hoffman and Rosen, 1981), generates a degree of spatial coherence in cardiac tissue although the estimated size of organized patches is much smaller than the scale of the heart.

The spatial correlation C_0 used by Bayly et al. (1993b) is sensitive only to correlations between simultaneous events and the correlation between sites exhibiting similar activity at different times was underestimated. However, the estimated correlation length suggested that a large number of small reentrant circuits coexisted simultaneously on the ventricular surface during their experiments. Thus, the use of C_0 to estimate the overall spatial correlation and averaging the results over the 2π space angle was appropriate to extract a scalar correlation length. This approach may not be suitable, however, for atrial fibrillation. High–density mapping experiments in patients (Konings et al., 1994) demonstrated that electrically induced AF is a heterogeneous arrhythmia characterized by different numbers and dimensions of atrial epicardial reentrant circuits. The complexity observed in right atrial activation maps ranged from relatively simple patterns (type I) where single uniformly propagating, broad fibrillation waves were activating the mapping electrode, to highly fragmented complex patterns (type III) characterized by the presence of multiple reentering wavelets.

Therefore, in the present analysis, the association length was estimated along the short and long principal axis of the iso–correlation contours to account for the spatial anisotropy in correlation maps of sustained AF. We defined a surface of association $S_a = \pi \times$short axis length$\times$ long axis length of the e^{-1} contour (Table 1) to obtain a rough estimate of the spatial extension

of coherent atrial patches. To calculate S_a, the redundancy I_{m} was used as an overall measure of spatial organization. Hence, during sustained AF, the average surface of association was $S_a \simeq \pi \times 0.9 \times 1.6 = 4.5$ cm^2 in the left atrium and $S_a \simeq \pi \times 1.5 \times 3.2 = 15.0$ cm^2 in the right atrium, respectively. The right atrial area S_a may actually be regarded as a lower bound, since the long principal axis in the right atrium often exceeded the border of the mapping electrode (3.2 cm). If S_a is interpreted as the average spatial domain covered by a single fibrillation wavelet, this suggests that the mapping electrode (area 9 cm^2) was visited on average by approximately two wavelets in the left atrium and by one in the right atrium. These findings are consistent with the results reported by Hoekstra et al. (1997) which characterized the AF dynamics of local electrograms in the same population of goats using nonlinear methods. The results suggested that sustained AF was of an intermediate level of complexity (type II), in which the mapped area is activated by one or two fibrillation waves most of the time.

Taking the total surface area of the atria equal to about 45 cm^2 in the goat, the estimated area S_a suggests that during sustained AF the average number of dynamically independent regions was about five ($\frac{22.5}{4.5} = 5$) in the left atrium and between one and two ($\frac{22.5}{15.0} = 1.5$) in the right atrium. If the number of independent atrial regions is associated with the number of independent wavelets, about seven fibrillation waves were present on the atrial surface during sustained AF, which is in agreement with the observation that four to six wavelets are needed on average for the perpetuation of AF (Allessie et al., 1985). We note that the correlation length has been used to estimate the number of independent surface waves (about seventy) during fully developed VF (Bayly et al., 1993b; Egolf and Greenside, 1994), which is about an order of magnitude larger than the estimated number of epicardial wavelets (about seven) present during sustained AF. This difference in apparent complexity has been attributed to the two dimensional nature of AF, while VF may be considered essentially three dimensional. The role of three dimensional wave propagation and the influence of myocardial wall thickness on the initiation and maintenance of ventricular fibrillation has not yet been settled conclusively (Gray et al., 1995; Winfree, 1994). Recent evidence from atrial mapping experiments (Gray et al., 1996; Holm et al., 1997; Schüssler et al., 1993) suggests that the complex three dimensional anatomy of the atria, in particular the network of pectinate muscles, may play an important role in activation during AF (Gray and Jalife, 1998; Wu et al., 1998).

The correlation length during AF in humans was estimated from the spatial cross correlation of sequences of local activation times constructed from bipolar electrograms recorded from a decapolar catheter located in the right atrium (Botteron and Smith, 1995). The peak of the cross correlation was identified, which is similar to the procedure to calculate C_{m}. The correlation length was termed the activation space constant, being the distance over which activation sequences remained well correlated. The correlation length ranged from 17 to 42 mm in patients with paroxysmal AF. In patients with chronic AF the activation space constant was 14 to 22 mm (Botteron and Smith, 1996), which is similar to the right atrial short axis correlation length estimated from C_{m} during sustained AF in the five goats (Table 1). However, their results were not related to the spatial complexity of AF and smaller correlation lengths may be expected in patterns where the degree of macroscopic organization is governed by many reentering wavelets, like for instance during fully developed AF (type III). For instance, a correlation length of 5 to

10 mm was reported during AF in a patient with chronic heart disease (Sih et al., 1995).

Interpretation of Association Length

To serve as a reference, we briefly mention some known intrinsic length scales in cardiac tissue. During the depolarization phase of the cardiac action potential transmembrane current flows outward into the intracellular space. The distance over which these electrotonic currents flow is a function of the coupling of myocardial cells. The electrotonic decay length is about 1 mm and is termed the space constant for cardiac tissue (Witkowski et al., 1992; Witkowski et al., 1995). Volume conduction effects resulting from electrical sources diminish as the inverse distance squared to the source, and may extend over several centimeters. For example, far field effects from ventricular activation are picked up by unipolar electrodes positioned at the atrial surface. To suppress a bias in the atrial spatial correlation a coherent averaging procedure was applied in this study to eliminate ventricular deflections in locally recorded unipolar atrial electrograms during AF. The electrotonic component becomes negligible with respect to volume conduction at distances larger than about five space constants (Witkowski et al., 1995). Furthermore, a sufficient amount of tissue is necessary to inject enough current into surrounding cells so that propagation of the cardiac action potential is maintained and the safety factor for conduction (the ratio between generated excitatory current and the current required for excitation) remains larger than one. The extension of this region is termed the liminal length (Arnsdorf and Sawicki, 1996; Starmer, 1997) and is about 0.2 to 0.4 mm (Winfree, 1991; Winfree, 1993).

It is an important issue how to connect different types of observable pattern correlation lengths to the characteristic physical length scale of the dynamics and to obtain a physiological interpretation of the correlation length. In this respect it is important to address the question whether detailed ionic models are needed or that a satisfactory description of the activation pattern can be given in macroscopic terms. Since currently it is not feasible to perform whole heart simulations with ionic models, reentry is often studied from the macroscopic perspective. For instance, Moe's computer model of AF (Moe et al., 1964) was used to study spatial organization and the correlation length was related to quantities like refractory period and local conduction velocity (Peck et al., 1994). Organization enhanced with increasing tissue wavelength (the product of conduction velocity times refractory period, equivalent to the minimum path length for reentry in the leading circle model) and the correlation length was interpreted as the radius of the spatial domain covered by a fibrillation wave during leading circle reentry (Botteron and Smith, 1995).

The surface of association S_a defined in this study is interpreted as the area covered by a coherent patch of fibrillating atrial tissue, which may correspond to the extension of the spatial domain of a fibrillation wavelet. We hypothesize that S_a is a measure of the number of independent wavelets on the epicardial atrial surface, and that larger association lengths result from fewer and larger reentrant circuits. Since the association length is estimated from a nonlinear statistic which characterizes the underlying dynamics, it seems particularly suited to characterize spatial coupling in activation patterns generated by the process of chronic atrial fibrillation. It should be noted that the different definitions of the correlation length and association length

would result in an estimation of about four times as much wavelets for the spatial redundancy compared to the spatial correlation function in atria of fixed size, identifying the estimated area of coherence with the spatial domain covered by a fibrillation wavelet. Considering the values of the correlation and association length at $\tau_{\max}$ for sustained AF (Table 1, the difference is about a factor $\sqrt{2}$), we estimate roughly twice as many wavelets for the spatial redundancy, indicating a deviation from a multivariate linear Gaussian random process.

High–resolution mapping experiments in dogs demonstrated that it is possible to locally entrain the atrial free wall during electrically induced AF by means of rapid atrial pacing (Kirchhof et al., 1993). In these dogs AF was spontaneously terminating, but the selected episodes of AF lasted longer than 15 minutes. The atrial activation pattern of AF was classified as type II and the area of the controlled region during atrial capture was approximately 16 cm^2, which is similar to the right atrial area of association S_a estimated during sustained AF in the population of goats. Thus, the maximum extent of the region that can be entrained by local rapid atrial pacing may correspond to the size of a coherent patch of epicardial myocardium which can be considered dynamically uncoupled from the remainder of the atrium.

Sih and colleagues reported that iso–correlation contours in coherence maps of fibrillation were irregularly shaped (Sih et al., 1995). They mentioned that anisotropic conductivity of the extracellular fluids could be a possible cause for this irregularity. It was suggested this would likely make the contours elliptical in case of random spatial activation, and that the additional irregularities which they observed in the contours demonstrated spatial organization of AF. In general, in this study the contours in correlation maps are more or less elliptical shaped. We surmise that the stretching of the contours is not caused by anisotropic conduction of randomly wandering wavelets, but that it is caused by fibrillation waves traversing the mapped region following a more or less constant course of activation. This seemed to be the case especially in the right atrial free wall, where the contours were rather elongated or cigar shaped (cf. Fig. 4). Visual inspection of the course of activation through animation of propagating wavefronts by sequentially displaying snapshots of the activation pattern (dynamic display, see also (KenKnight et al., 1995; Lee et al., 1996; Rogers et al., 1998)) revealed that the long principal axis of the contours was oriented parallel to the average orientation of activation wavefronts, while the short principal axis pointed in the average direction of the propagation (perpendicular to the wavefront). Therefore, the activation pattern during sustained AF seemed rather organized consisting of predominantly uniformly conducting, broad fibrillation waves activating the right atrial free wall. Left atrial correlation maps (cf. Fig. 6) also indicated a main direction of propagation for AF wavelets. However, the estimated association lengths (Table 2) were smaller than in the right atrium, which suggests that the left atrial activation pattern was less organized.

Limitations of the Study

In the nonlinear correlation analysis several parameters had to be chosen to estimate the redundancy and it is unknown how to choose them optimally with regards to the characterization of cardiac activation patterns. The choices made were previously motivated by Hoekstra et al. (1997) who characterized the dynamics of sustained AF by a nonlinear analysis of single local

electrograms in the same five goats.

To reduce spatial correlation introduced by atrial pickup of far field electrical activity, ventricular deflections were removed from local atrial electrograms by coherent averaging of the ventricular complex. The results of this procedure depend on the visual selection of a suitable time window around the R wave in a ventricular epicardial lead to calculate a template of the far field ventricular activity. Coherent averaging may not be optimal to eliminate far field effects, but it is a relatively simple procedure and visual inspection showed that ventricular potentials were effectively removed from the atrial electrograms.

Conclusions

To understand the macroscopic mechanisms of atrial fibrillation it is necessary to accurately describe the activation pattern in time and space. The correlation analysis of atrial activation patterns serves to get some insight into the features essential to include in a mathematical description. In this study both linear and nonlinear correlation measures were applied to characterize spatial organization during sustained AF. It was demonstrated that nonlinear spatial coupling was present mainly in right atrial activation patterns of sustained AF.

Up to date, it remains controversial to what extent fibrillation is organized (Bayly et al., 1998; Gray et al., 1998; Jalife et al., 1998) and in which aspects atrial fibrillation is different from ventricular fibrillation (Gray and Jalife, 1998). High–density mapping has revealed that AF is characterized by a spectrum of varying fibrillation cycle lengths and a various degree of complexity of activation patterns generated by different types of reentry (Allessie et al., 1996a; Allessie et al., 1996b; Konings et al., 1994). Furthermore, it has been shown that some degree of temporal and spatial organization exists during the early stages of VF (Bayly et al., 1993b; Clayton et al., 1995; Huang et al., 1998; Lee et al., 1996; Witkowski et al., 1998). Mapping studies showed that reentry during VF in the intact heart is characterized by multiple, small reentrant circuits (Janse et al., 1995; Pogwizd and Corr, 1990; Witkowski and Penkoske, 1990) but also persists in the presence of only a few reentrant waves in two dimensional ventricular preparations (Janse et al., 1995). Even a single, rapidly moving reentrant wave may constitute a simple form of fibrillation in normal ventricular myocardium (Gray et al., 1995). By now it has become clear, that fibrillation is a heterogeneous arrhythmia which may manifest itself through temporal organization (i.e. periodicity observed in local electrograms) resulting from spatial disorder (i.e. many coexisting wavelets), as well as through temporal disorder created by a relatively high degree of underlying spatial organization.

The correlation analysis presented here pointed out that the activation pattern of sustained AF in goats was relatively organized (type II) with nonlinear coupling extending over a distance of 8 to 15 mm. Spatial anisotropy observed in correlation maps was taken into account and the two principal directions of spatial organization were considered separately. The size of a coherent patch of atrial tissue during AF was estimated as the surface of association spanned by the short and long principal axis of the spatial redundancy, which may represent the spatial domain of a fibrillation wavelet. We surmise that it is a measure of the number of independent wavelets present in the atria during sustained AF, and that larger association lengths result

from fewer and larger reentrant circuits.

ACKNOWLEDGMENTS

This study was supported by grant no. 805-06-181 from the Council for Earth and Life Sciences (ALW), which is subsidized by the Netherlands Organization for Scientific Research (NWO). We thank Jan VanderSchoot for stimulating discussions about the singular value decomposition.

REFERENCES

Allessie, M. A., Bonke, F. I. M., and Schopman, F. J. G. (1977): Circus movement in rabbit atrial muscle as a mechanism of tachycardia III. The "leading circle" concept: a new model of circus movement in cardiac tissue without the involvement of an anatomical obstacle. *Circ. Res. 41*: 9–18.

Allessie, M. A., Kirchhof, C. J. H. J., and Konings, K. T. S. (1996a): Unraveling the electrical mysteries of atrial fibrillation. *Eur. Heart J. 17*: (suppl. C), 2–9.

Allessie, M. A., Konings, K. T. S., Kirchhof, C. J. H. J., and Wijffels, M. C. E. F. (1996b): Electrophysiological mechanisms of perpetuation of atrial fibrillation. *Am. J. Cardiol. 77*: 10A–23A.

Allessie, M. A., Lammers, W. J. E. P., Bonke, F. I. M., and Hollen, J. (1985): Experimental evaluation of Moe's multiple wavelet hypothesis of atrial fibrillation In Zipes, D. P. and Jalife, J., editors, *Cardiac electrophysiology and arrhythmias* pp: 265–275. Grune and Stratton New York.

Arnsdorf, M. O. and Sawicki, G. J. (1996): Flecainide and the electrophysiologic matrix: the effects of flecainide acetate on the determinants of cardiac excitability in sheep purkinje fibers. *J. Cardiovasc. Electrophysiol. 7*: 1172–1182.

Bayly, P. V., Johnson, E. E., Idriss, S. F., Ideker, R. E., and Smith, W. M. (1993a): Efficient electrode spacing for examining spatial organization during ventricular fibrillation. *IEEE Trans. Biomed. Eng. 40*: 1060–1066.

Bayly, P. V., Johnson, E. E., Wolf, P. D., Greenside, H. S., Smith, W. M., and Ideker, R. E. (1993b): A quantitative measurement of spatial order in ventricular fibrillation. *J. Cardiovasc. Electrophysiol. 4*: 533–546.

Bayly, P. V., KenKnight, B. H., Rogers, J. M., Johnson, E. E., Ideker, R. E., and Smith, W. M. (1998): Spatial organization, predictability, and determinism in ventricular fibrillation. *Chaos 8*: 103–115.

Botteron, G. W. and Smith, J. M. (1995): A technique for measurement of the extent of spatial organization of atrial activation during atrial fibrillation in the intact human heart. *IEEE Trans. Biomed. Eng. 42*: 579–586.

Botteron, G. W. and Smith, J. M. (1996): Quantitative assessment of the spatial organization of atrial fibrillation in the intact human heart. *Circulation 93*: 513–518.

Chan, K.-S. (1997): On the validity of the method of surrogate data In Cutler, C. D. and Kaplan, D. T., editors, *Nonlinear Dynamics and Time Series. Building a bridge between the natural and statistical sciences* volume 11 of *Fields Inst. Communications* pp: 77–97. American Math. Soc. Providence, Rhode Island.

Clayton, R. H., Murray, A., and Campbell, R. W. F. (1995): Evidence for electrical organization during ventricular fibrillation in the human heart. *J. Cardiovasc. Electrophysiol. 6*: 616–624.

Cox, J. L., Canavan, T. E., Schüssler, R. B., Cain, M. E., Lindsay, B. D., Stone, C., Smith, P. K., Corr, P. B., and Boineau, J. P. (1991): The surgical treatment of atrial fibrillation. II. Intraoperative electrophysiologic mapping and description of the electrophysiological basis of atrial flutter and atrial fibrillation. *J. Thorac. Cardiovasc. Surg. 101*: 406–426.

Damle, R. S., Kanaan, N. M., Robinson, N. S., Ge, Y.-Z., Goldberger, J. J., and Kadish, A. H. (1992): Spatial and temporal linking of epicardial activation directions during ventricular fibrillation in dogs. Evidence for underlying organization. *Circulation 86*: 1547–1558.

Eckmann, J.-P. and Ruelle, D. (1985): Ergodic theory of chaos and strange attractors. *Rev. Mod. Phys. 57*: 617–656.

Egolf, D. A. and Greenside, H. S. (1994): Relation between fractal dimension and spatial correlation length for extensive chaos. *Nature 369*: 129–131.

Fraser, A. M. (1989): Reconstructing attractors from scalar time series: A comparison of singular system and redundancy criteria. *Physica D 34*: 391–404.

Gerstenfeld, E. D., Sahakian, A. V., and Swiryn, S. (1992): Evidence for transient linking of atrial excitation during atrial fibrillation in humans. *Circulation 86*: 375–382.

Grassberger, P. (1988): Finite sample corrections to entropy and dimension estimates. *Phys. Lett. A 128*: 369–373.

Grassberger, P. and Procaccia, I. (1983): Estimation of the Kolmogorov entropy from a chaotic signal. *Phys. Rev. A 28*: 2591–2593.

Gray, R. A. and Jalife, J. (1996): Spiral waves and the heart. *Int. J. of Bifurcation and Chaos 6*(3): 415–435.

Gray, R. A. and Jalife, J. (1998): Ventricular fibrillation and atrial fibrillation are two different beasts. *Chaos 8*: 65–78.

Gray, R. A., Jalife, J., Panfilov, A. V., Baxter, W. T., Cabo, C., Davidenko, J. M., and Pertsov, A. M. (1995): Mechanisms of cardiac fibrillation. *Science 270*: 1222–1225.

Gray, R. A., Pertsov, A. M., and Jalife, J. (1996): Incomplete reentry and epicardial breakthrough patterns during atrial fibrillation in the sheep heart. *Circulation 94*: 2649–2661.

Gray, R. A., Pertsov, A. M., and Jalife, J. (1998): Spatial and temporal organization during cardiac fibrillation. *Nature 392*(6671): 75–78.

Hoekstra, B. P. T., Diks, C. G. H., Allessie, M. A., and DeGoede, J. (1997): Nonlinear analysis of the pharmacological conversion of sustained atrial fibrillation in conscious goats by the class Ic drug cibenzoline. *Chaos 7*: 430–446.

Hoffman, B. F. and Rosen, M. R. (1981): Cellular mechanisms for cardiac arrhythmias. *Circ. Res. 49*: 1–15.

Holm, M., Johansson, R., Brandt, J., Lührs, C., and Olsson, S. B. (1997): Epicardial right atrial free wall mapping in chronic atrial fibrillation. Documentation of repetitive activation with a focal spread – a hitherto unrecognised phenomenon in man. *Eur. Heart J. 18*: 290–310.

Huang, J., Rogers, J. M., KenKnight, B. H., Rollins, D. ., Smith, W. M., and Ideker, R. E. (1998): Evolution of the organization of epicardial activation patterns during ventricular fibrillation. *J. Cardiovasc. Electrophysiol. 9*: 1291–1304.

Ikeda, T., Uchida, T., Hough, D., Lee, J. J., Fishbein, M. C., Mandel, W. J., Chen, P.-S., and Karagueuzian, H. S. (1996): Mechanism of spontaneous termination of functional reentry in isolated canine right atrium. Evidence for the presence of an excitable but nonexcited core. *Circulation 94*: 1962–1973.

Jalife, J., Berenfeld, O., Skanes, A., and Mandapati, R. (1998): Mechanisms of atrial fibrillation: Mother rotors or multiple daughter wavelets or both? *J. Cardiovasc. Electrophysiol. 9*: S2–S12.

Jalife, J. and Gray, R. (1996): Drifting vortices of electrical waves underlie ventricular fibrillation in the rabbit heart. *Acta Physiol. Scand. 157*: 123–131.

Janse, M. J., Wilms-Schopman, F. J. G., and Coronel, R. (1995): Ventricular fibrillation is not always due to multiple wavelet reentry. *J. Cardiovasc. Electrophysiol. 6*: 512–521.

KenKnight, B. H., Bayly, P. V., Gerstle, R. J., Rollins, D. L., Wolf, P. D., Smith, W. M., and Ideker, R. E. (1995): Regional capture of fibrillating ventricular myocardium. Evidence of an excitable gap. *Circ. Res. 77*: 849–855.

Kirchhof, C. J. H. J., Chorro, F., Scheffer, G. J., Brugada, J., Konings, K., Zetelaki, Z., and Allessie, M. A. (1993): Regional entrainment of atrial fibrillation studied by high–resolution mapping in open–chest dogs. *Circulation 88*: 736–749.

Konings, K. T. S., Kirchhof, C. J. H. J., Smeets, J. R. L. M., Wellens, H. J. J., Penn, O. C., and Allessie, M. A. (1994): High–density mapping of electrically induced atrial fibrillation in humans. *Circulation 89*: 1665–1680.

Konings, K. T. S., Smeets, J. R. L. M., Penn, O. C., Wellens, H. J. J., and Allessie, M. A. (1997): Configuration of unipolar atrial electrograms during electrically induced atrial fibrillation in humans. *Circulation 95*: 1231–1241.

Lee, J. J., Kamjoo, K., Hough, D., Hwang, C., Fan, W., Fishbein, M. C., Bonometti, C., Ikeda, T., Karagueuzian, H. S., and Chen, P.-S. (1996): Reentrant wave fronts in Wiggers' stage II ventricular fibrillation: Characteristics, and mechanisms of termination and spontaneous regeneration. *Circ. Res. 78*: 660–675.

Moe, G. K. (1962): On the multiple wavelet hypothesis of atrial fibrillation. *Arch. Int. Pharmacodyn. Ther. 140*: 183–188.

Moe, G. K., Rheinboldt, W. C., and Abildskov, J. A. (1964): A computer model of atrial fibrillation. *Am. Heart J. 67*: 200–220.

Ortiz, J., Nawano, S., Abe, H., Rudy, Y., Johnson, N. J., and Waldo, A. L. (1994): Mapping the conversion of atrial flutter to atrial fibrillation and atrial fibrillation to atrial flutter. Insights into mechanisms. *Circ. Res. 74*: 882–894.

Paluš, M. (1995): Testing for nonlinearity using redundancies: Quantitative and qualitative aspects. *Physica D 80*(1-2): 186–205.

Paluš, M. (1996): Detecting nonlinearity in multivariate time series. *Phys. Lett. A 213*: 138–147.

Paluš, M., Albrecht, V., and Dvorák, I. (1993): Information–theoretic tests for nonlinearity in time series. *Phys. Lett. A 175*: 203–209.

Paluš, M. and Novotna, D. (1994): Testing for nonlinearity in weather records. *Phys. Lett. A 193*: 67–74.

Pawelzik, K. and Schuster, H. G. (1987): Generalized dimensions and entropies from a measured time series. *Phys. Rev. A 35*: 481–484.

Peck, J. B., Bayly, P. V., Botteron, G. W., and Smith, J. M. (1994): The effects of refractoriness and conduction velocity on spatial organization in a computer model of atrial fibrillation. *Computers in Cardiol.* pp: 237–240.

Pogwizd, S. M. and Corr, P. B. (1990): Mechanisms underlying ventricular tachycardia and fibrillation in the ischemic heart: Relation to nonlinear dynamics In Jalife, J., editor, *Mathematical approaches to cardiac arrhythmias* volume 591 of *Ann. N. Y. Acad. Sci.* pp: 278–300. New York Acad. Sci. New York.

Pompe, B., Blidh, P., Hoyer, D., and Eiselt, M. (1998): Using mutual information to measure coupling in the cardiorespiratory system. New insights into nonlinear coordinations. *IEEE Eng. Med. Biol. Magaz. 17*: 32–39.

Prichard, D. and Theiler, J. (1994): Generating surrogate data for time series with several simultaneously measured variables. *Phys. Rev. Lett. 73*: 951–954.

Prichard, D. and Theiler, J. (1995): Generalized redundancies for time series analysis. *Physica D 84*: 476–493.

Rapp, P. E., Albano, A. M., Zimmerman, I. D., and Jimenez-Montano, M. A. (1994): Phase–randomized surrogates can produce spurious identifications of non–random structure. *Phys. Lett. A 192*: 27–33.

Rogers, J. M., Bayly, P. V., Ideker, R. E., and Smith, W. M. (1998): Quantitative techniques for analyzing high–resolution cardiac–mapping data. *IEEE Eng. Med. Biol. Magaz. 17*: 62–72.

Roithinger, F. X., SippensGroenewegen, A., Karch, M. R., Steiner, P. R., Ellis, W. S., and Lesh, M. D. (1998): Organized activation during atrial fibrillatin in man: Endocardial and electrocardiographic manifestations. *J. Cardiovasc. Electrophysiol. 9*: 451–461.

Ropella, K. M., Baerman, J. M., Sahakian, A. V., and Swiryn, S. (1990): Differentation of ventricular arrhythmias. *Circulation 82*: 2035–2043.

Ropella, K. M., Sahakian, A. V., Baerman, J. M., and Swiryn, S. (1989): The coherence spectrum. A quantitative discriminator of fibrillatory and nonfibrillatory cardiac rhythms. *Circulation 80*: 112–119.

Sahakian, A. V., Ropella, K. M., Baerman, J. M., and Swiryn, S. (1990): Measuring the organization of cardiac rhythms using the magnitude–squared coherence function. *IEEE Eng. Med. Biol. Magaz. 9*: 25–28.

Schreiber, T. and Schmitz, A. (1996): Improved surrogate data for nonlinearity tests. *Phys. Rev. Lett. 77*(4): 635–638.

Schüssler, R. B., Kawamoto, T., Hand, D. E., Mitsuno, M., Bromberg, B. I., Cox, J. L., and Boineau, J. P. (1993): Simultaneous epicardial and endocardial activation sequence mapping in the isolated canine right atrium. *Circulation 88*: 250–263.

Sih, H. J., Sahakian, A. V., Arentzen, C. E., and Swiryn, S. (1995): A frequency domain analysis of spatial organization of epicardial maps. *IEEE Trans. Biomed. Eng. 42*: 718–727.

Sih, H. J., Zipes, D. P., Berbari, E. J., and Olgin, J. E. (1999): A high–temporal resolution algorithm for quantifying organization during atrial fibrillation. *IEEE Trans. Biomed. Eng. 46*: 440–450.

Slocum, J., Sahakian, A., and Swiryn, S. (1988): Computer discrimination of atrial fibrillation and regular atrial rhythms from intra–atrial electrograms. *Pacing Clin. Electrophysiol. 11*: 610–621.

Stam, C. J., Pijn, J. P. M., and Pritchard, W. S. (1998): Reliable detection of nonlinearity in experimental time series with strong periodic components. *Physica D 112*(3-4): 361–380.

Starmer, C. F. (1997): The cardiac vulnerable period and reentrant arrhythmias: Targets of anti– and proarrhythmic processes. *Pacing Clin. Electrophysiol. 20*: 445–454.

Takens, F. (1983): Invariants related to dimensions and entropy. *Atas do 13. Coloquio Brasileiro de Matemat.* pp: 353–359.

Theiler, J., Eubank, S., Longtin, A., Galdrikian, B., and Farmer, J. D. (1992a): Testing for nonlinearity in time series: the method of surrogate data. *Physica D 58*: 77–94.

Theiler, J., Galdrikian, B., Longtin, A., Eubank, S., and Farmer, J. D. (1992b): Using surrogate data to detect nonlinearity in time series In Casdagli, M. and Eubank, S., editors, *Nonlinear modeling and forecasting, Santa Fe Institute studies in the sciences of complexity, Proc. Vol. 12* pp: 163–188. Addison–Wesley, Reading Mass.

Theiler, J., Linsay, P. S., and Rubin, D. M. (1993): Detecting nonlinearity in data with long coherence times In Weigend, A. S. and Gershenfeld, N. A., editors, *Time series prediction: Forecasting the future and understanding the past, Santa Fe Institute studies in the sciences of complexity, Proc. Vol. 15* pp: 429–455. Addison–Wesley Reading Mass.

Theiler, J. and Prichard, D. (1996): Constrained–realization Monte–Carlo method for hypothesis testing. *Physica D 94*: 221–235.

Theiler, J. and Prichard, D. (1997): Using "surrogate surrogate data" to calibrate the actual rate of false positives in tests for nonlinearity in time series In Cutler, C. D. and Kaplan, D. T., editors, *Nonlinear Dynamics and Time Series. Building a bridge between the natural and statistical sciences* volume 11 of *Fields Inst. Communications* pp: 99–113. American Math. Soc. Providence, Rhode Island.

van der Stappen, M. L. M., Schouten, J. C., and van den Bleek, C. M. (1994): The gas–solids fluidized bed as a spatio-temporal chaotic system. *Proc. of the 1st international particle technology forum, Part I, Denver, USA* pp: 446–451.

Wells, J. L., Karp, R. B., Kouchoukos, N. T., MacLean, W. A. H., James, T. N., and Waldo, A. L. (1978): Characterization of atrial fibrillation in man: Studies following open heart surgery. *Pacing Clin. Electrophysiol. 1*: 426–438.

Wijffels, M. C. E. F., Dorland, R., Mast, F., and Allessie, M. A. (2000): Widening of the excitable gap during pharmacological cardioversion of atrial fibrillation in the goat. *Circulation 102*: 260–267.

Wijffels, M. C. E. F., Kirchhof, C. J. H. J., Dorland, R., and Allessie, M. A. (1995): Atrial fibrillation begets atrial fibrillation. A study in awake chronically instrumented goats. *Circulation 92*: 1954–1968.

Winfree, A. T. (1991): Estimating the ventricular fibrillation threshold In Glass, L., Hunter, P., and McCulloch, A., editors, *Theory of heart. Biomechanics, biophysics and nonlinear dynamics of cardiac function* pp: 477–532. Springer–Verlag New York.

Winfree, A. T. (1993): How does ventricular tachycardia decay into ventricular fibrillation? In Shenasa, M., Borggrefe, M., and Breithardt, G., editors, *Cardiac mapping* pp: 655–680. Futura Armonk, New York.

Winfree, A. T. (1994): Electrical turbulence in three–dimensional heart muscle. *Science 266*: 1003–1006.

Witkowski, F. X., Kavanagh, K. M., Penkoske, P. A., and Plonsey, R. (1995): Epicardial cardiac source–field behavior. *IEEE Trans. Biomed. Eng. 42*: 552–558.

Witkowski, F. X., Leon, L. J., Penkoske, P. A., Giles, W. R., Spano, M. L., Ditto, W. L., and Winfree, A. T. (1998): Spatiotemporal evolution of ventricular fibrillation. *Nature 392*: 78–81.

Witkowski, F. X. and Penkoske, P. A. (1990): Activation patterns during ventricular fibrillation In Jalife, J., editor, *Mathematical approaches to cardiac arrhythmias* volume 591 of *Ann. N. Y. Acad. Sci.* pp: 219–231. New York Acad. Sci. New York.

Witkowski, F. X., Penkoske, P. A., and Kavanagh, K. M. (1992): Estimate of electromotive surface dimension during ventricular fibrillation. *Proc. IEEE Eng. Med. Biol. Conference* pp: 631–632.

Wu, T.-J., Yashima, M., Xie, F., Athill, C. A., Kim, Y.-H., Fishbein, M. C., Qu, Z., Garfinkel, A., Weiss, J. N., Karagueuzian, H. S., and Chen, P.-S. (1998): Role of pectinate muscle bundles in the generation and maintenance of intra–atrial reentry. Potential implications for the mechanism of conversion between atrial fibrillation and atrial flutter. *Circ. Res. 83*: 448–462.